

Overview

Biomedical Applications of Fluorescence Imaging In Vivo

Moinuddin Hassan, PhD¹ and Brenda A. Klaunberg, VMD^{2,*}

Optical imaging can advance knowledge of cellular biology and disease at the molecular level in vitro and, more recently, in vivo. In vivo optical imaging has enabled real-time study to track cell movement, cell growth, and even some cell functions. Thus, it can be used in intact animals for disease detection, screening, diagnosis, drug development, and treatment evaluation. This review includes a brief introduction to fluorescence imaging, fluorescent probes, imaging devices, and in vivo applications in animal models. It also describes a quantitative fluorescence detection method with a reconstruction algorithm for determining the location of fluorophores in tissue and addresses future applications of in vivo fluorescence imaging.

The recent increase in animal models, driven by genetic engineering, emphasizes the need for better methods to evaluate these valuable animals. Traditional assessment typically relies on post-mortem tissue collection and analysis at various time points. This approach often requires large numbers of animals. The development of specialized imaging devices such as magnetic resonance imaging (MRI) and computerized tomography (CT) facilitate non-invasive visualization of internal organs, thereby reducing the number of animals required to achieve research objectives. For example, one can follow the pathophysiology of disease in an individual animal and observe the relationship of the lesion to the other organ systems in an intact biological system. This attribute can lead to a better understanding of disease processes, including detection of novel events and relationships.

MRI (68, 73) and CT (41, 64) are excellent tools for three-dimensional imaging. Although it is possible to perform some functional analysis, these methods are somewhat limited by the size of the imaging target in a living animal. Fluorescence reporter genes and cell markers, in contrast, permit microscopic examination of specific molecular events such as intracellular activity, gene expression, and cell movement or growth. Fluorescence was used historically for in vitro studies such as cell culture assays, cell imaging, and tissue staining, but recently it has been extended to in vivo imaging. Its application in living animals is useful to validate in vitro data and enhance our understanding of in vivo events. The use of fluorescence for in vivo optical imaging is not only non-invasive, it provides images in "real time," and offers rapid data acquisition times (seconds to minutes). While optical imaging equipment is simple and inexpensive compared to MR, and most optical markers appear to be non-toxic,

there are also unique challenges and limitations to this technique, which we will discuss. Nevertheless, in vivo fluorescence imaging is expected to have a significant impact on animal-based research. As the specificity of probes increase, quantification theories improve, and three-dimensional localization becomes more robust, the clinical application of in vivo fluorescence imaging may one day enhance surgical biopsy with in vivo optical guidance, thereby decreasing the probability of false-negative results.

Light and Fluorescence

Light is a form of energy in units called "photons" and results from excitation of electrons. There are different ways to excite electrons. Examples of light generated by thermal energy include sunlight, fire, and electric lightbulbs. Chemical reactions can produce "cold light" such as the light of "glow sticks" and the bioluminescence produced by fireflies and other organisms. Light itself can excite electrons, and this is how fluorescence is generated. The visible spectrum of photon wavelengths ranges from 400 (violet) to 700 nm (red). Light exists at wavelengths above (infrared) and below (ultraviolet) the visible spectrum, but the human eye is unable to see those wavelengths.

When a fluorescence molecule (fluorophore) absorbs a photon, electrons in its outer shell are excited and lifted from a ground state to an excited state. Upon return to the ground state they release energy, which is detected as fluorescence. Fluorescence is a cyclic process, unless the fluorophore is destroyed irreversibly in the excited state (photobleaching). The emitted photon has less energy and consequently a longer wavelength than the initially absorbed photon, resulting in a color shift. For example, rhodamine absorbs green light (520 to 565 nm) and emits red light (625 to 740 nm). The wavelength of the released photon is determined by Planck's constant and depends on the energy released by an electron as it returns to its ground state. The emitted wavelength is longer than the absorbed wavelength if single photons are absorbed. The difference between the absorbed and emitted wavelength is called Stokes shift. The energy difference is absorbed as heat within the atomic lattice of the material. The

Received: 11/08/04. Revision requested: 11/19/04. Accepted: 11/22/04.

¹Laboratory of Integrative and Medical Biophysics, National Institute of Child Health and Human Development, National Institutes of Health, Building 9 Room B1E11, Bethesda, Maryland 20892; ²Mouse Imaging Facility, National Institute of Neurological Disorders and Stroke, National Institutes of Health, 10 Center Drive, B1D-69, Bethesda, Maryland 20892-1060.

*Corresponding author.

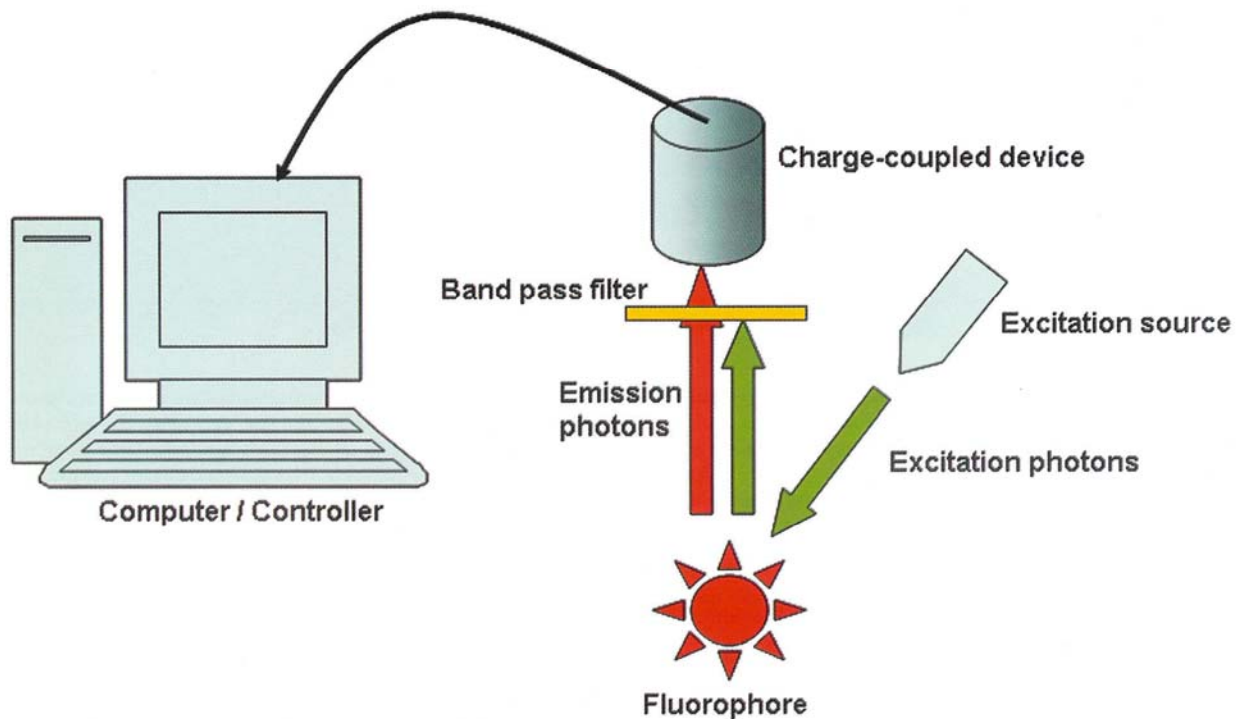


Figure 1. A schematic diagram of a fluorescence imaging set-up.

Stokes shift and spectral bandwidth of fluorescence molecules for *in vivo* fluorescence imaging must be known to meet detector requirements. Flexibility in experimental design is also needed to avoid overlapping incident and emission wavebands. Because there may be overlapping wavelengths of the probe and other fluorophores, we can specify a narrow emission filter wavelength to exclude the unwanted signal. Fluorescence has been used to study molecular interaction in cell biology (75), physiology (33), cardiology (66), analytical chemistry (50), biochemistry (72), and environmental science (51). During the past five years, its popularity has increased greatly with the development of new fluorescence compounds, software, detection devices, and quantitative methods.

Fluorescence Imaging Technology

Four components are required for an *in vivo* fluorescence imaging system: a) a fluorescent probe, b) an excitation source, c) a filter to isolate emission and excitation light, and d) a detector that captures emitted light and produces a recordable electrical signal or photographic image. The detector must be sensitive but have low noise sensitivity and the ability to detect wavelengths for a given application. The most widely used detector system is a charge-coupled device (CCD) camera (5, 39, 40, 63). A low-noise image is obtained by using long exposures; however, as exposure length is increased, the effect of thermal noise begins to dominate the signal. Therefore, CCD cameras are usually available with a thermo-electric cooler. A photomultiplier tube (PMT) also can be used as a detector (62). A PMT can measure very weak light because it multiplies the effect of emitted light and converts photons into electrical signals so that the light can be pre-

cisely measured. A schematic diagram of a fluorescence imaging setup is shown in Fig. 1.

Selection of an appropriate optical filter is another important issue for fluorescence intensity detection. A filter is used to specify the excitation and emission wavelength band. To increase the sensitivity of a detector system, filter characteristics should permit transmission of at least 95% of the desired fluorescence signal. Detection sensitivity is severely affected by background noise that may originate from unbound or nonspecifically bound probes (reagent background) or from endogenous sources (autofluorescence). Selecting an emission filter with a narrow bandwidth can minimize autofluorescence or reagent background noise. The filter blocks the wavelengths outside the desired range, and increases the sensitivity for overall fluorescence intensity detection.

Fluorophores

Superior fluorescent probes are essential for successful fluorescence imaging. A fluorophore is a molecule that is naturally occurring or specially designed. A fluorophore can be used as a probe to label cells or tissues. Probes can be designed or selected to localize to tissues or cells or to respond to a specific stimulus. Probes can also be used to localize proteins within a cell or to monitor the production of a gene product (11). Probes can be bound to an antibody for delivery to specific targets. The most common naturally occurring fluorophore proteins emit fluorescent light in the green or red wavelengths. Examples include green fluorescence protein (GFP), red fluorescence protein (RFP), and rhodamine. Fluorophores also have been engineered to address specific research aims by utilizing different wave-

lengths. For deep-tissue imaging, fluorophores with higher excitation and emission wavelengths, especially those in the near-infrared (NIR) region (650 to 1000 nm), have significant advantages because they have lower scattering properties in tissue and lower absorption in blood and water. The choice of fluorophore is dependent on the application and target. The factors that influence the choice of fluorophore include availability and stability of the probe, target tissue depth, and anatomical location. An example of how a fluorophore can be used to target a specific cell function is described in Bremer (7). Their model fluoresces when a chemical bond in the fluorophore is cleaved. Bremer also demonstrated that fluorescence occurred when the target fluorophore underwent conformational changes after interaction with a specific enzyme (8).

Green Fluorescent Protein

GFP is a naturally fluorescing protein found in a jellyfish (*Aequorea victoria*) (61). Sunlight does not travel far in seawater, so the jellyfish also contains a bioluminescence protein, called *acqorin*, which produces blue light. The fluorescence protein GFP absorbs the blue light produced by the bioluminescence at a wavelength of 470 nm and emits green light at a wavelength of about 510 nm. GFP has been used to measure human tumor development and metastasis in small-animal cancer models including ovarian (12, 76), lung (15, 59, 77), prostate (54), melanoma (57), pancreatic (5, 6), brain (78), and breast (52, 65) cancer. It is also possible to use GFP in any application where fluorescent cell labeling is desired; examples include gene expression (70), viral infection (1, 34), and embryonic development (53). A sample image of GFP in vivo can be seen in Fig. 2. GFP does not require a substrate to fluoresce and does not appear to interfere with cell growth or function.

RFP from *Discosoma* coral has different properties than GFP (32, 55). RFP is excited at 558 nm and has peak emission at 583 nm. RFP may become a useful tool for in vivo imaging because of its lower scattering and absorption in the tissue at these wavelengths. The signal of RFP is distinct from that of GFP and is, therefore, ideal for co-labeling of tissue.

Near-Infrared Fluorophores

NIR fluorophores can be naturally occurring (such as RFP), but most are chemically engineered to fluoresce in the near-infrared ranges. The higher emission wavelengths of NIR make them ideal for deep-tissue imaging with low tissue absorption. NIR fluorophores have been used to track labeled cells in vivo in cancer research. Cells can be labeled with fluorescent antibodies, or other techniques, depending on the application (3). Applications include cancer typing, response to treatment, tracking drug metabolism, and localizing tumors and measuring their size and growth rate or metastasis. Cypate-mono-2-deoxy-glucose is a NIR fluorescence contrast agent and has been used to label glycolysis for the localization of mouse tumors (13). Tumors generally have an increased basal metabolic rate, and glycolysis is higher in the tumor than surrounding tissue. A dye-peptide conjugate, such as cyanine-peptide, is another type of NIR fluorescent dye chemically bound to a target molecule and has the potential to target specific tumors, assess drug delivery, and monitor treatment in animal models (3, 10, 69). Another kind of fluorescence dye, indocyanine dye (Cy5.5), is widely used for fluorescence imaging. Cy5.5-antibody conjugates have been used effec-

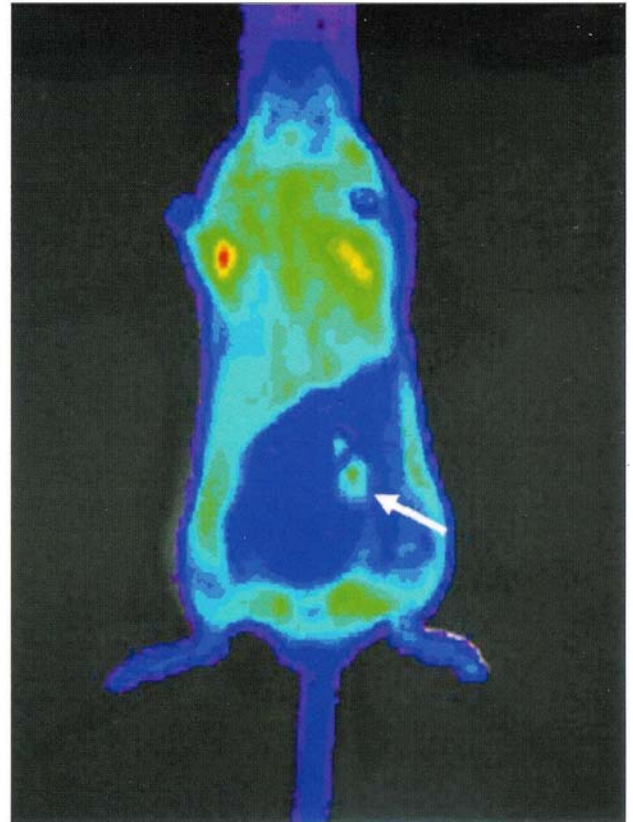


Figure 2. GFP-expressing urogenital tumor injected subcutaneously (arrow) in a mouse. Note the autofluorescence on the haired areas, the hair around the tumor site was clipped. Image acquired with the IVIS Imaging System (Xenogen Corp., Alameda, Calif.). Courtesy of Dr. James Vasselli and Dr. W. Marston Linehan, National Cancer Institute.

tively to visualize tumors. A Cy5.5-conjugated biocompatible protected graft copolymer (PGC) has been used to investigate therapeutic drug development within tumor microvasculature (4). Citrin and colleagues (16, 17) also developed a mouse model to detect tumor vasculature. They labeled endostatin, a potent inhibitor of angiogenesis, with Cy5.5 and determined that it can selectively localize to a tumor. The data showed that endostatin-Cy5.5 localized to the tumor in a dose-dependent manner, as shown in Fig. 3.

NIR fluorophores have also been used to monitor biological processes such as thrombin activity. For example, Cy5.5 conjugated to a thrombin-specific oligopeptide substrate has been used to image thrombin activity in a mouse model of experimental thrombosis (42). In a similar context, a factor XIIIa-sensitive NIR fluorescence probe has been used to image factor XIIIa activity during experimentally induced thrombosis (43). Finally, Hansch and colleagues reported recently that antigen-induced rheumatoid arthritis in mice can be visualized by anti-F4/80 monoclonal antibodies labeled with Cy5.5 (36).

Quantum Dots

Semiconductor quantum dots (QDs) are nanometer (1 to 10 nm)-sized crystals that have been covalently linked to biorecognition molecules such as peptides, antibodies, nucleic acids, or small molecules for application as fluorescence probes

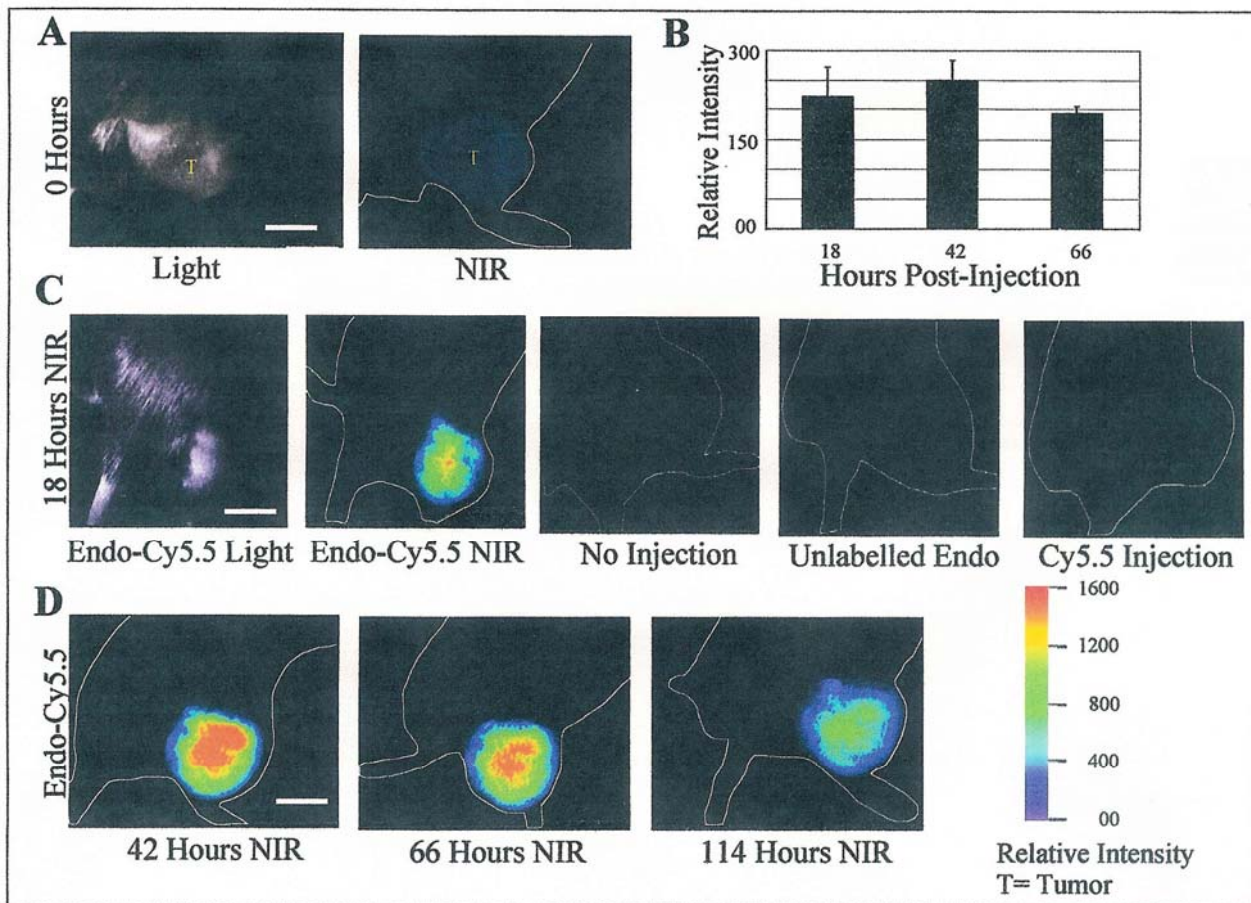


Figure 3. Imaging results from four C57BL/6 mice (16). (A) Images of a mouse implanted with Lewis lung carcinoma in a previously shorn area that received no injection, unlabeled endostatin, or Cy5.5 alone. (B) Quantification of the average relative intensity of the endostatin-Cy5.5 signal at 18 h (n = 6), 42 h (n = 4), and 66 h (n = 3). (C) Near-infrared images of mice that received endostatin-Cy5.5, no injection, endostatin alone, or Cy5.5 dye alone at 18 h. (D) Near-infrared signal generated from a mouse that was injected with endostatin-Cy5.5 at 42, 66, and 114 h. The signal peaks at 42 h but is present at 114 h. A relative intensity profile is shown at the right.

(9, 18, 19, 45, 49, 74). Limitations of organic fluorophores include broad spectral overlap, photobleaching, and poor water solubility. Compared with organic fluorophores, QDs have unique optical and electronic properties, including tunable fluorescence emission from the visible to infrared wavelength and large absorption coefficients across a wide spectral range. QDs are available in single or multicolored forms. Multicolored QDs can have the same excitation wavelength but will fluoresce at different emission wavelengths. Multicolored QDs can be used for detection of multiple molecular targets by excitation with a single light source and detection of no or minimal spectral overlap. Therefore, different populations of cells are able to be imaged concurrently while bearing different colors (27). In addition, QDs have sustainable brightness and photostability, whereas organic dyes are photobleached quickly. Thus, QDs have significant advantages for continuous, extended, real-time imaging. QDs have hydrophilic properties, so they are soluble in aqueous buffers and sensitive to pH changes. This makes them useful for biological labeling of biofluids and metabolic processes in vivo (19, 35).

Toxicity is a current disadvantage of using QDs in vivo. There are indications that this drawback can be overcome and that biocompatible and nontoxic-coated nanocrystals can be used successfully for in vivo animal studies. Dubertret and colleagues (19) used encapsulated individual nanocrystals in phospholipid block-copolymer micelles to study the embryonic development of *Xenopus*, whereas QDs with polydentate phosphine coatings have been used effectively to localize lymph nodes in mice (47). Recently, polyethylene glycol (PEG)-coated QDs conjugated to an antibody against the prostate-specific membrane antigen have been used successfully to target image human prostate cancer in a mouse model (28).

Limitations of Fluorescence Imaging In Vivo

The signals used for optical imaging are subject to physical limitations inherent to light. Signals are emitted in all directions; some photons are scattered, while others are absorbed, but only those reaching the detector are recorded. Hair can impede this path, but clipping and depilatories may help. Pigmented

skin also may impede the signal path to the detector, so many investigators use non-pigmented, hairless mice for these reasons. Detection of light from deep tissues can be aided by repositioning the animal so that the site of interest is closer to the detector. If the signal is still deep or too weak, it may be necessary to employ different imaging techniques.

The signals generated during *in vivo* fluorescence imaging are low compared to more common light sources such as fireflies or flashlights. The detectors are sensitive to low-light emissions, but it is imperative that the animal does not move during imaging. Immobility can be accomplished through general anesthesia. Fluorescence imaging is a painless procedure, but general anesthesia offers the best method of preventing the animal from experiencing stress due to restraint. In addition, the muscle tone of an anesthetized animal is relaxed, thus permitting optimal positioning for imaging.

Many tissues autofluoresce and may interfere with signal detection, especially of a weak signal. Collagens, for example, fluoresce in the lower visible wavelengths. Some of the more commonly used markers such as GFP also fluoresce within this range (490 to 515 nm). There is no easy way to avoid autofluorescence when imaging *in vivo*. Some intestinal autofluorescence may be due to dietary chlorophyll. Rodent diets low in alfalfa have been shown to decrease autofluorescence. As mentioned earlier, clipping hair may help to decrease surface autofluorescence. Probes that have higher excitation and emission wavelengths are advantageous because there is less autofluorescence interference in the infrared ranges. Also, there is deeper tissue penetration with wavelengths > 600 nm. New methods to overcome deep signal detection and autofluorescence interference are being developed (28, 58). Therefore, a tunable wavelength filter and “unmixing” of the signal spectrum help to minimize the autofluorescence and improve visualization.

Quantitative Fluorescence Imaging

Quantification of signal is useful for localizing a tumor in three dimensions; this helps to determine the size, volume, and depth of the lesion. The most common fluorescence imaging devices record the spatial intensity distribution of fluorescence emission qualitatively. A typical two-dimensional (2-D) image is shown in Fig. 4. The fluorescence intensity distribution, as an image observed at the tissue surface, is dependent on the concentration of the fluorophores at the site, the optical properties of the tissue, and the location of the fluorophores. To quantify the embedded fluorophore detected at the tissue surface, knowledge of photon paths from within the tissue is required.

Because of the nature of optical imaging, signal quantification and three-dimensional (3-D) image reconstruction is a challenging task. One method that is being investigated for quantification of optical data is tomography. With tomography, multiple emission sources and detectors surround the region of interest in order to collect data from multiple points. Tomographic methods have shown some promise; however, a theoretical approach using typical 2-D image data is an alternative, and various theories to quantify signal have been developed (13, 30). A robust quantitative theory of diffuse fluorescence imaging is discussed in the following section. In addition, an animal model to investigate the immune response to tumor, using the theory, is also presented.

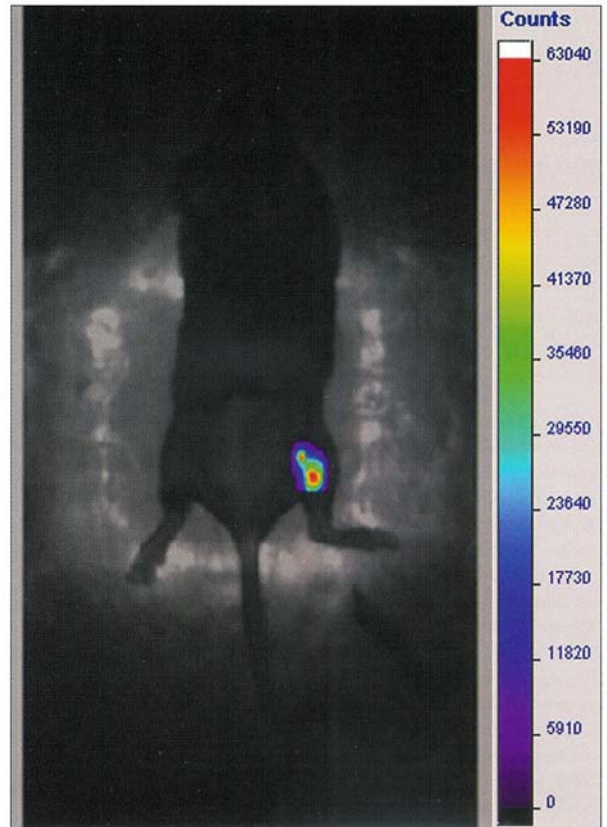


Figure 4. A two-dimensional intensity distribution of a fluorescence image obtained from a mouse tumor by using a SAMI system (Advance Research Technologies, Inc., Saint-Laurent, Quebec, Canada).

Theory and 3-D Reconstruction Algorithm

The theory of quantitative diffuse fluorescence photon migration is based on the Random Walk Theory (RWT) (2). In the RWT model, the description of a photon path may be divided into three parts, and each part can be described by a probability. The first part is the path from the photon source to a target, and the probability is that an incident photon will arrive at the fluorophore site. The second part is the interaction of the photon with the fluorophore, the probability of which depends on at least two factors. The first factor is the probability that the photon will have a reactive encounter with the fluorophore. This probability incorporates the corresponding photon transit delay, which is dependent on the lifetime of the fluorophore. The second factor is the probability that the fluorophore will emit a photon. The third part of photon path description is the probability that the photon will travel from the reaction site to the detector. Each of these parts is governed by a stochastic process.

An analytical expression was derived for continuous wave (CW) imaging in the reflectance mode (21, 22). The probability of detecting an emitted photon $[\Gamma(r, s)]$ originating at the deeply embedded fluorophore is given by a random walk formula (14, 22):

1)

$$\Gamma(r, s) = \frac{\Phi \frac{\mu_{af}}{\mu_{sf}} [H(\alpha_i, \beta_i) - H(\alpha_e, \beta_e) - H(\alpha_i, \beta_i) + H(\alpha_e, \beta_e)] \exp(-\frac{\mu_{ae}}{\mu_{ae}})}{\left\{ 1 - \frac{\mu_{af}}{\mu_{sf}} + \frac{\mu_{af}}{\mu_{sf}} \left[1 + \frac{1}{8} \left(\frac{2}{\pi} \right) \sum_{m=1}^{\infty} \frac{1}{m^2} \exp(-2m \frac{\mu_{af}}{\mu_{sf}}) \right] \right\}}$$

where:

$$2) \quad H(\alpha, \beta) = \frac{1}{\sqrt{\alpha\beta}} \exp\left\{-2 \left[\sqrt{\alpha} \frac{\mu_{af}}{\mu_{sf}} + \sqrt{\beta} \frac{\mu_{ae}}{\mu_{ae}} \right]\right\}$$

$$3) \quad \alpha_{\pm} = \frac{3}{4} \left[x_f^2 + y_f^2 + (z_f \pm \frac{\sqrt{2}}{\mu_{ae}})^2 \right] \mu_{sf}^2$$

and

$$4) \quad \beta_{\pm} = \frac{3}{4} \left[(x_f - \bar{x})^2 + (y_f - \bar{y})^2 + (z_f + \frac{\sqrt{2}}{\mu_{ae}} \pm \frac{\sqrt{2}}{\mu_{ae}})^2 \right] \mu_{ae}^2$$

Here, the origin of the coordinate system (0,0,0) is placed at the entry point of the incident photon, and the coordinates of the fluorescent site and the detector are $(\bar{x}_f, \bar{y}_f, \bar{z}_f)$ and $(\bar{x}, \bar{y}, \bar{z})$, respectively. The optical parameters in this equation, μ_{sf}' and μ_{ae} , are the background's transport-corrected scattering and absorption coefficients, respectively. The subscripts *i* and *e* stand for incident and emitted light, respectively. Symbols μ_{sf}' and μ_{af} represent the optical characteristics (the transport-corrected scattering and absorption coefficients, respectively) of the fluorescent site. The quantum efficiency, Φ , is the probability that an excited fluorophore will, in fact, emit a fluorescent photon. It should be noted that for several fluorescent sites, the detected signal can be considered as the sum of the signals arising from individual fluorophores.

The next step in the development of the 3-D reconstruction algorithm is to devise an inverse algorithm that enables one to locate the fluorescent mass in vivo and determine its concentration. The observed 2-D intensity distributions of the emitted light were normalized to the maximum intensity measured in the mouse tumor and used as input data for 3-D localization of the target (26).

The analysis was based on a comparison of measured fluorescent intensity distributions with the theoretical expression for the probability $\Gamma(r, s)$ (Eq. 1) that corresponds to the intensity distribution of the light emitted by a fluorophore embedded at a given depth. Parameters, μ_{sf}' and μ_{af} , and the whole denominator of the right-hand side of Eq. 1 are not required for the reconstruction because they determine only the scaling of the intensities.

The algorithm uses a multi-parameter curve-fitting procedure, based on a standard Levenberg-Marquardt method (38). The 2-D problem is reduced to 1-D using a single variable $w = (x/s)n_{sc} + y/s$ which characterizes the position of the pixel on the image plane, where *s* is the distance between neighboring pixels and is the number of pixels in each linear scan (e.g., $n_{sc} = 512$ for a square image field of 512×512 pixels). The strong dependence of the intensity distributions (given by Eq. 1) on the fluorophore depth contributes to the robustness of the algorithm (14). This algorithm has been tested in well-defined phantoms (24).

Animal Model of Quantitative Fluorescence Imaging

To validate the reconstruction algorithm, Gannot and colleagues developed a model in tumor-bearing mice that demonstrated accurate 3-D reconstruction of a fluorescence signal originating from a depth of ≤ 2 mm (26). Mice were first injected in the tongue with 10^5 murine squamous cell carcinoma cells. It

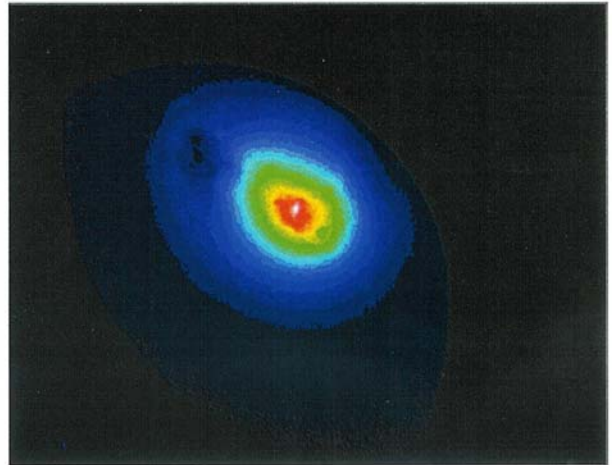


Figure 5. In vivo surface fluorescence image of a murine squamous cell carcinoma in a mouse tongue labeled with fluoresceinated antibody.

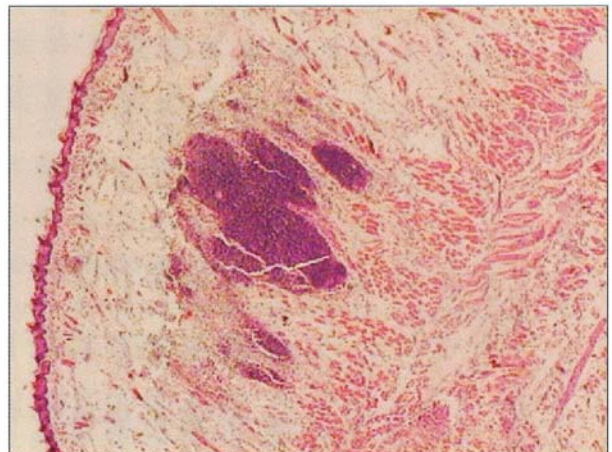


Figure 6. A 2-day-old murine squamous cell carcinoma in a mouse tongue. H&E stain, magnification $\times 2$.

was previously shown that this tumor line attracts CD3+ and CD19+ lymphocytes (23), so the fluorophore fluorescein isothiocyanate (FITC) was conjugated to anti-CD3 and anti-CD19 antibodies for imaging the tumor locations. At various times up to 20 days after cell-line injection, a sub-group of mice was injected into the tongue with either anti-CD3-FITC or anti-CD19-FITC conjugates.

In order to simulate the location of tumors at various depths ≤ 2 mm, a slab of agarose gel, with optical properties similar to human tissue, was placed on each tongue for imaging. Excitation of the fluorophores was produced by an argon laser at 488 nm, and emission was limited to wavelengths between 520 to 550 nm. A single fluorescent object was detected through the agarose in the tumor area of the tongue, and the 2-D image is shown in Fig. 5. Immediately after imaging, tongue biopsies were prepared for histology, and the measured depth was compared to the calculated depth. Fig. 6 is a hematoxylin- and eosin-stained tongue section from a diseased mouse 2 days after injection of the cell line.

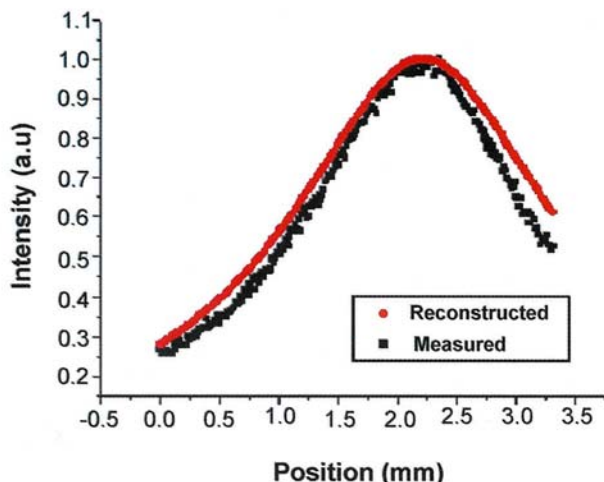


Figure 7. Comparison of intensity profiles from a mouse tumor, with profiles reconstructed from the theoretical model (taken at day 2) for $z_f = 1.18$ mm nominal thickness of the turbid layer above the mouse tongue with fluorophore and antibody. The reconstructed depth is 1.09 mm.

In order to calculate the tumor depth based on the emission intensity, the theory was applied. Using the integrating spheres method (24), initial values for the background optical parameters (μ_{si}' , μ_{ai} and μ_{se}' , μ_{ae} at the excitation and emission wavelengths) were chosen from the obtained measurements of total reflectance and transmittance. A comparison of the detected intensity profiles, with the profiles reconstructed from the theoretical model, is shown in Fig. 7. The data showed that the calculated tumor depth was close to the actual measured depth, with error margins between 8.7% and 16.6%. As one would expect, the deeper tumors were more difficult to calculate accurately because of more photon scattering.

The pharmacokinetics of fluorophore–antibody complexes in the vicinity of the tumor is also important for imaging. The binding specificity of tumor antigens with labeled antibodies and those fluorophores that may diffuse away from the tumor site must be considered. Gannot and colleagues (25) investigated these factors and their influence on deep-tissue optical imaging. They used the same fluorophore–antibody conjugate described in the preceding paragraphs. A series of fluorescence images was taken, and a cross-sectional slice through the peak fluorescence intensity showed the broadening of the fluorescence signal as a function of time. Reconstructed (deconvolved) peak intensities were estimated as inversely proportional to the squared width of the corresponding concentration profile. Figure 8 is an example of fluorescence peak intensity (measure and deconvolved) as a function of time to show the actual exponential clearance of fluoresceinated antibodies in the vicinity of a mouse tongue tumor.

Future Applications of In Vivo Fluorescence

The lifetime (time for an electron to return from excited state to initial state) of a fluorophore can vary in response to changes in the immediate environment such as temperature, pH, tissue oxygen content, nutrient supply, and bioenergetic status (48). The heterogeneity in tumor vascularity can be seen as indicated by changes in pH and temperature (71). These changes can be

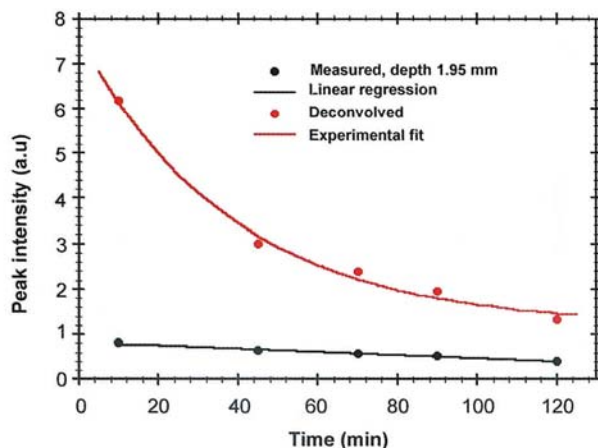


Figure 8. Clearance time, as seen through an agarose slab and deconvolved to show actual exponential clearance.

useful for the prognosis of malignancies and to develop techniques for drug targeting.

The pH range in normal tissue is 7.2 to 7.6, but many solid tumors exhibit a pH value that can be as low as 5.6 (31). The average decrease in tumor pH is 0.3 to 0.5 pH units. When pH measurements were taken in various studies performed in animal models of human tumors (20, 46), they revealed a positive correlation between tumor size and the decrease in pH.

Localized temperatures can also vary with neoplastic processes. Tumor temperature can be 0.5 to 4.0° C higher than that of the normal tissue (37.0° C) (29, 37, 60). In addition, the temperature response of neoplastic tissue during hyperthermia differs from that of normal tissue (44). A positive correlation was observed between temperature differences and degree of angiogenesis when the thermal response between malignant tumors and benign inflammatory lesions was investigated (67).

Fluorophore lifetime imaging is a promising tool for early detection of tumors. By selecting fluorophores with known lifetime dependence on specific environmental variables, researchers may be able to localize the metabolic parameters using optical imaging, as well as identify changes in local molecular concentration in vivo.

Confocal fluorescence microscopy traditionally was used for in vitro studies; however, new technology is extending its use in vivo. A confocal microscope is designed to use the focal point of the lens to help create the best image, while filtering signals outside of the focal point. When combined with fiber optics, it enhances visualization of biological processes in vivo (fiber optic fluorescence microendoscopy). Thus, flexible probes can be inserted into various cavities or placed at a tissue surface to image cellular activity. Fiber optic fluorescence microendoscopy recently was used to visualize individual neurons and red blood cell dynamics in the rat brain (56). This technique also can be used to visualize microvessel diameters, vasoconstriction or dilation, and circulating cells and nerve fiber bundles (Fig. 9).

Summary

Fluorescence imaging in vivo utilizes naturally occurring or synthesized fluorophores to visualize intracellular activity and cell movement in living animals. A wide range of optical markers is available, including GFP, RFP, NIR fluorophores, and QDs. Al-

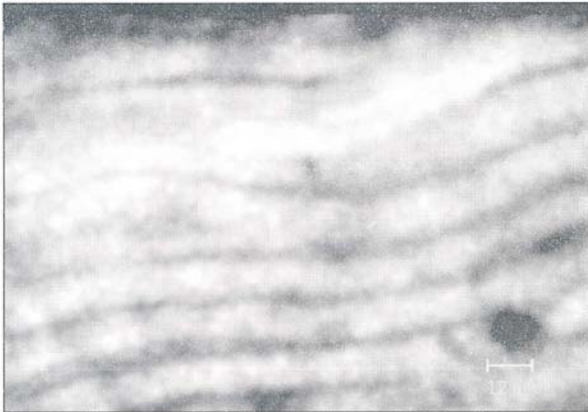


Figure 9. Fluorescence labeling of rat sciatic nerve in vivo. Image was acquired with the Cell-viZio system (Mauna Kea Technologies, Paris, France) at 2.5- μ m resolution after injection of fluorescent membrane dye. The optic fiber was placed directly on the sciatic nerve in order to visualize the sensory and the motor fibers bundles. Courtesy of Galit Pelled (National Institute of Neurological Disorders and Stroke).

though fluorescence markers generally appear to be safe for in vivo use and although they usually do not interfere with normal cell metabolism, the toxicity of QD nanocrystals is not yet completely understood. Fluorescence imaging has proven especially useful for characterization of cancer cells and metastatic lesions, but it also has been applied to the examination of subcellular functions such as gene expression and enzymatic activity.

Some of the technical obstacles of fluorescence imaging are beginning to be overcome through new technological advances that refine the signal-to-noise ratio and improve the quality of the data produced. These new methods also offer better ways to quantitate signal intensity and depth, which may lead to the use of in vivo fluorescence imaging for optical enhancement of surgical biopsy in clinical practice. In addition, new imaging devices allow for the study of fluorescence lifetime in response to metabolic conditions, which may lead to early tumor detection. The combined use of confocal microscopy and fiber optics also offers promise for fluorescence imaging at the cellular level in living tissue. In vivo optical imaging is an emerging and powerful tool with a multitude of potential uses for basic research and clinical diagnostics.

Acknowledgments

We thank Amir H. Gandjbakhche and Israel Gannot (Laboratory of Integrative and Medical Biophysics, National Institutes of Child Health and Human Development) for their valuable suggestions and helpful discussions. We also thank Kevin Camphausen (National Cancer Institute), Anthony Durkin (Bechman Laser Institute) and Paul D. Smith (Office of the Director, National Institutes of Health) for their support. The views, opinions, and findings contained in this review are those of the authors and do not reflect official policy or positions of the U. S. Department of Health and Human Services, the National Institutes of Health, or the United States Government.

References

1. **Agungpriyono, D. R., R. Yamaguchi, K. Uchida, Y. Tohya, A. Kato, Y. Nagai, M. Asakawa, and S. Tateyama.** 2000. Green fluorescent protein gene insertion of Sendai Virus infection in nude mice: possibility as an infection tracer. *J. Vet. Med. Sci.* **62**:223-228.

2. **Arridge, S. R. and J. C. Hebden.** 1997. Optical imaging in medicine: II. Modelling and reconstruction. *Phys. Med. Biol.* **42**:841-853.
3. **Becker, A., C. Hesseus, K. Licha, B. Ebert, U. Sukowski, W. Semmler, B. Wiedenmann, and C. Grotzinger.** 2001. Receptor-targeted optical imaging of tumors with near-infrared fluorescent ligands. *Nat. Biotechnol.* **19**:327-331.
4. **Bogdanov, A. A., Jr., C. P. Lin, M. Simonova, L. Matuszewski, and R. Weissleder.** 2002. Cellular activation of the self-quenched fluorescent reporter probe in tumor microenvironment. *Neoplasia* **4**:228-236.
5. **Bouvet, M., J. Wang, S. R. Nardin, R. Nassirpour, M. Yang, E. Baranov, P. Jiang, A. R. Moossa, and R. M. Hoffman.** 2002. Real-time optical imaging of primary tumor growth and multiple metastatic events in a pancreatic cancer orthotopic model. *Cancer Res.* **62**:1534-1540.
6. **Bouvet, M., M. Yang, S. Nardin, X. Wang, P. Jiang, E. Baranov, A. R. Moossa, and R. M. Hoffman.** 2000. Chronologically-specific metastatic targeting of human pancreatic tumors in orthotopic models. *Clin. Exp. Metastasis* **18**:213-218.
7. **Bremer, C., S. Bredow, U. Mahmood, R. Weissleder, and C. H. Tung.** 2001. Optical imaging of matrix metalloproteinase-2 activity in tumors: feasibility study in a mouse model. *Radiology* **221**:523-529.
8. **Bremer, C., V. Ntziachristos, and R. Weissleder.** 2003. Optical-based molecular imaging: contrast agents and potential medical applications. *Eur. Radiol.* **13**:231-243.
9. **Bruchez, M., Jr., M. Moronne, P. Gin, S. Weiss, and A. P. Alivisatos.** 1998. Semiconductor nanocrystals as fluorescent biological labels. *Science* **281**:2013-2016.
10. **Bugaj, J. E., S. Achilefu, R. B. Dorshow, and R. Rajagopalan.** 2001. Novel fluorescent contrast agents for optical imaging of in vivo tumors based on a receptor-targeted dye-peptide conjugate platform. *J. Biomed. Opt.* **6**:122-133.
11. **Chalfie, M., Y. Tu, G. Euskirchen, W. W. Ward, and D. C. Prasher.** 1994. Green fluorescent protein as a marker for gene expression. *Science* **263**:802-805.
12. **Chaudhuri, T. R., J. M. Mountz, B. E. Rogers, E. E. Partridge, and K. R. Zinn.** 2001. Light-based imaging of green fluorescent protein-positive ovarian cancer xenografts during therapy. *Gynecol Oncol.* **82**:581-589.
13. **Chen, Y., G. Zheng, Z. H. Zhang, D. Blessington, M. Zhang, H. Li, Q. Liu, L. Zhou, X. Intes, S. Achilefu, and B. Chance.** 2003. Metabolism-enhanced tumor localization by fluorescence imaging: in vivo animal studies. *Opt. Lett.* **28**:2070-2072.
14. **Chernomordik, V., D. Hattery, I. Gannot, and A. H. Gandjbakhche.** 1999. Inverse method 3-D reconstruction of localized in vivo fluorescence—application to Sjogren syndrome. *IEEE Quantum Electron.* **5**:930-935.
15. **Chishima, T., Y. Miyagi, X. Wang, Y. Tan, H. Shimada, A. Moossa, and R. M. Hoffman.** 1997. Visualization of the metastatic process by green fluorescent protein expression. *Anticancer Res.* **17**:2377-2384.
16. **Citrin, D., A. K. Lee, T. Scott, M. Sproull, C. Menard, P. J. Tofilon, and K. Camphausen.** 2004. In vivo tumor imaging in mice with near-infrared labeled endostatin. *Mol. Cancer Ther.* **3**:481-488.
17. **Citrin, D., T. Scott, M. Sproull, C. Menard, P. J. Tofilon, and K. Camphausen.** 2004. In vivo tumor imaging using near-infrared-labeled endostatin molecule. *Int. J. Radiation Oncology Biol. Phys.* **58**:536-541.
18. **Dahan, M., S. Levi, C. Luccardini, P. Rostaing, B. Riveau, and A. Triller.** 2003. Diffusion dynamics of glycine receptors revealed by single-quantum dot tracking. *Science* **302**:442-445.
19. **Dubertret, B., P. Skourides, D. J. Norris, V. Noireaux, A. H. Brivanlou, and A. Libchaber.** 2002. In vivo imaging of quantum dots encapsulated in phospholipid micelles. *Science* **298**:1759-1762.
20. **Engin, K., D. B. Leeper, J. R. Cater, A. J. Thistlethwaite, L. Tupchong, and J. D. McFarlane.** 1995. Extracellular pH distribution in human tumors. *Int. J. Hyperthermia* **11**:211-216.
21. **Gandjbakhche, A. H., R. F. Bonner, R. Nossal, and G. H. Weiss.** 1997. Effects of multiple-passage probabilities on fluorescent signals from biological media. *Appl. Opt.* **36**:4613-4619.

22. **Gandjbakhche, A. H. and I. Gannot.** 1996. Quantitative fluorescent imaging of specific markers of diseased tissue. *IEEE Quantum Electron.* **2**:914-921.
23. **Gannot, G., I. Gannot, H. Vered, A. Buchner, and Y. Keisari.** 2002. Increase in immune cell infiltration with progression of oral epithelium from hyperkeratosis to dysplasia and carcinoma. *Br. J. Cancer* **86**:1444-1448.
24. **Gannot, I., R. F. Bonner, G. Gannot, P. C. Fox, P. D. Smith, and A. H. Gandjbakhche.** 1998. Optical simulations of a noninvasive technique for the diagnosis of diseased salivary glands in situ. *Med. Phys.* **25**:1139-1144.
25. **Gannot, I., A. Garashi, V. Chernomordik, and A. Gandjbakhche.** 2004. Quantitative optical imaging of the pharmacokinetics of fluorescent-specific antibodies to tumor markers through tissuelike turbid media. *Opt. Lett.* **29**:742-744.
26. **Gannot, I., A. Garashi, G. Gannot, V. Chernomordik, and A. Gandjbakhche.** 2003. In vivo quantitative three-dimensional localization of tumor labeled with exogenous specific fluorescence markers. *Appl. Opt.* **42**:3073-80.
27. **Gao, X., W. C. Chan, and S. Nie.** 2002. Quantum-dot nanocrystals for ultrasensitive biological labeling and multicolor optical encoding. *J. Biomed. Opt.* **7**:532-537.
28. **Gao, X., Y. Cui, R. M. Levenson, L. W. Chung, and S. Nie.** 2004. In vivo cancer targeting and imaging with semiconductor quantum dots. *Nat. Biotechnol.* **22**:969-976.
29. **Gautherie, M.** 1980. Thermopathology of breast cancer: measurement and analysis of in vivo temperature and blood flow. *Ann. N.Y. Acad. Sci.* **335**:383-413.
30. **Graves, E. E., R. Weissleder, and V. Ntziachristos.** 2004. Fluorescence molecular imaging of small animal tumor models. *Curr. Mol. Med.* **4**:419-430.
31. **Griffiths, J. R.** 1991. Are cancer cells acidic? *Br. J. Cancer* **64**:425-427.
32. **Gross, L. A., G. S. Baird, R. C. Hoffman, K. K. Baldrige, and R. Y. Tsien.** 2000. The structure of the chromophore within DsRed, a red fluorescent protein from coral. *Proc. Natl. Acad. Sci. USA* **97**:11990-11995.
33. **Guth, K. and R. Wojciechowski.** 1986. Perfusion cuvette for the simultaneous measurement of mechanical, optical and energetic parameters of skinned muscle fibres. *Pflügers Arch.* **407**:552-527.
34. **Haan, K. M., A. Aiyar, and R. Longnecker.** 2001. Establishment of latent Epstein-Barr virus infection and stable episomal maintenance in murine B-cell lines. *J. Virol.* **75**:3016-3020.
35. **Haidekker, M. A., T. P. Brady, S. H. Chalian, W. Akers, D. Lichlyter, and E. A. Theodorakis.** 2004. Hydrophilic molecular rotor derivatives-synthesis and characterization. *Bioorg. Chem* **32**:274-289.
36. **Hansch, A., O. Frey, D. Sauner, I. Hilger, M. Haas, A. Malich, R. Brauer, and W. A. Kaiser.** 2004. In vivo imaging of experimental arthritis with near-infrared fluorescence. *Arthritis Rheum.* **50**:961-967.
37. **Hassan, M., R. F. Little, A. Vogel, K. Aleman, K. Wyvill, R. Yarchoan, and A. H. Gandjbakhche.** 2004. Quantitative assessment of tumor vasculature and response to therapy in Kaposi's sarcoma using functional noninvasive imaging. *Technol. Cancer Res. Treat.* **3**:451-457.
38. **Henson, D. E., L. Ries, L. S. Freedman, and M. Carriaga.** 1991. Relationship among outcome, stage of disease, and histologic grade for 22,616 cases of breast-cancer: the basis for a prognostic index. *Cancer* **68**:2142-2149.
39. **Hildebrandt, I. J. and S. S. Gambhir.** 2004. Molecular imaging applications for immunology. *Clin. Immunol.* **111**:210-224.
40. **Honigman, A., E. Zeira, P. Ohana, R. Abramovitz, E. Tavor, I. Bar, Y. Zilberman, R. Rabinovsky, D. Gazit, A. Joseph, A. Panet, E. Shai, A. Palmon, M. Laster, and E. Galun.** 2001. Imaging transgene expression in live animals. *Mol. Ther.* **4**:239-249.
41. **Hopper, K. D., K. Singapuri, and A. Finkel.** 2000. Body CT and oncologic imaging. *Radiology* **215**:27-40.
42. **Jaffer, F. A., C. H. Tung, R. E. Gerszten, and R. Weissleder.** 2002. In vivo imaging of thrombin activity in experimental thrombi with thrombin-sensitive near-infrared molecular probe. *Arterioscler. Thromb. Vasc. Biol.* **22**:1929-1935.
43. **Jaffer, F. A., C. H. Tung, J. J. Wykrzykowska, N. H. Ho, A. K. Houg, G. L. Reed, and R. Weissleder.** 2004. Molecular imaging of factor XIIIa activity in thrombosis using a novel, near-infrared fluorescent contrast agent that covalently links to thrombi. *Circulation* **110**:170-176.
44. **Jain, R. K.** 1980. Temperature distributions in normal and neoplastic tissues during normothermia and hyperthermia. *N.Y. Acad. Sci.* **335**:48-62.
45. **Jaiswal, J. K., H. Mattoussi, J. M. Mauro, and S. M. Simon.** 2003. Long-term multiple color imaging of live cells using quantum dot bioconjugates. *Nat. Biotechnol.* **21**:47-51.
46. **Kallinowski, F. and P. Vaupel.** 1988. pH distributions in spontaneous and isografted rat tumors. *Br. J. Cancer* **58**:314-321.
47. **Kim, S., Y. T. Lim, E. G. Soltesz, A. M. De Grand, J. Lee, A. Nakayama, J. A. Parker, T. Mihaljevic, R. G. Laurence, D. M. Dor, L. H. Cohn, M. G. Bawendi, and J. V. Frangioni.** 2004. Near-infrared fluorescent type II quantum dots for sentinel lymph node mapping. *Nat. Biotechnol.* **22**:93-97.
48. **Lakowicz, J. R., H. Szmacinski, K. Nowaczyk, K. W. Berndt, and M. Johnson.** 1992. Fluorescence lifetime imaging. *Anal. Biochem.* **202**:316-330.
49. **Larson, D. R., W. R. Zipfel, R. M. Williams, S. W. Clark, M. P. Bruchez, F. W. Wise, and W. W. Webb.** 2003. Water-soluble quantum dots for multiphoton fluorescence imaging in vivo. *Science* **300**:1434-1436.
50. **Laurence, T. A. and S. Weiss.** 2003. Analytical chemistry. How to detect weak pairs. *Science* **299**:667-668.
51. **Legendre, L. and C. M. Yentsch.** 1989. Overview of flow cytometry and image analysis in biological oceanography and limnology. *Cytometry* **10**:501-510.
52. **Li, Y., M. Tondravi, J. Liu, E. Smith, C. C. Haudenschild, M. Kaczmarek, and X. Zhan.** 2001. Cortactin potentiates bone metastasis of breast cancer cells. *Cancer Res.* **61**:6906-6911.
53. **Lipp, M. and G. Muller.** 2004. Lymphoid organogenesis: getting the green light from RORgamma(t). *Nat. Immunol.* **5**:12-14.
54. **Maeda, H., T. Segawa, T. Kamoto, H. Yoshida, A. Kakizuka, O. Ogawa, and Y. Kakehi.** 2000. Rapid detection of candidate metastatic foci in the orthotopic inoculation model of androgen-sensitive prostate cancer cells introduced with green fluorescent protein. *Prostate* **45**:335-340.
55. **Matz, M. V., A. F. Fradkov, Y. A. Labas, A. P. Savitsky, A. G. Zarskiy, M. L. Markelov, and S. A. Lukyanov.** 1999. Fluorescent proteins from nonbioluminescent *Anthozoa* species. *Nat. Biotechnol.* **17**:969-73.
56. **Mehta, A. D., J. C. Jung, B. A. Flusberg, and M. J. Schnitzer.** 2004. Fiber optic in vivo imaging in the mammalian nervous system. *Curr. Opin. Neurobiol.* **14**:617-628.
57. **Moore, A., N. Sergeev, S. Bredow, and R. Weissleder.** 1998. A model system to quantify tumor burden in locoregional lymph nodes during cancer spread. *Invasion Metastasis* **18**:192-197.
58. **Ornberg, R. L., B. M. Woerner, and D. A. Edwards.** 1999. Analysis of stained objects in histological sections by spectral imaging and differential absorption. *J. Histochem. Cytochem.* **47**:1307-1314.
59. **Paris, S., C. Chauzy, N. Martin-Vandeleit, B. Delpuch, L. Thiberville, J. P. Martin, and M. Diarra-Mehrpour.** 1999. A model of spontaneous lung metastases visualised in fresh host tissue by green fluorescent protein expression. *Clin. Exp. Metastasis* **17**:817-822.
60. **Pierart, J., R. Burmeister, J. Steinberg, J. Schalper, and L. Cid.** 1990. Thermography in the differential diagnosis of phylloides tumour. *Br. J. Surg.* **77**:783-784.
61. **Prasher, D. C., V. K. Eckenrode, W. W. Ward, F. G. Prendergast, and M. J. Cormier.** 1992. Primary structure of the *Aequorea victoria* green-fluorescent protein. *Gene* **111**:229-233.
62. **Ramanujam, N., J. Chen, K. Gossage, R. Richards-Kortum, and B. Chance.** 2001. Fast and noninvasive fluorescence imaging of biological tissues in vivo using a flying-spot scanner. *IEEE Trans. Biomed. Eng.* **48**:1034-1041.
63. **Rice, B. W., M. D. Cable, and M. B. Nelson.** 2001. In vivo imaging of light-emitting probes. *J. Biomed. Opt.* **6**:432-440.
64. **Rockoff, S. D.** 1977. The evolving role of computerized tomography in radiation oncology. *Cancer* **39**:694-696.

65. Schmidt, C. M., S. L. Settle, J. L. Keene, W. F. Westlin, G. A. Nickols, and D. W. Griggs. 1999. Characterization of spontaneous metastasis in an aggressive breast carcinoma model using flow cytometry. *Clin. Exp. Metastasis* 17:537-544.
66. Sollott, S. J., B. D. Ziman, and E. G. Lakatta. 1992. Novel technique to load indo-1 free acid into single adult cardiac myocytes to assess cytosolic Ca²⁺. *Am. J. Physiol.* 262:H1941-1949.
67. Stefanadis, C., C. Chrysochoou, D. Markou, K. Petraki, D. B. Panagiotakos, C. Fasoulakis, A. Kyriakidis, C. Papadimitriou, and P. K. Toutouzas. 2001. Increased temperature of malignant urinary bladder tumors in vivo: the application of a new method based on a catheter technique. *J. Clin. Oncol.* 19:676-681.
68. Taylor, J. S., P. S. Tofts, R. Port, J. L. Evelhoch, M. Knopp, W. E. Reddick, V. M. Runge, and N. Mayr. 1999. MR imaging of tumor microcirculation: promise for the new millennium. *J. Magn. Reson. Imaging* 10:903-907.
69. Tung, C. H. 2004. Fluorescent peptide probes for in vivo diagnostic imaging. *Biopolymers* 76:391-403.
70. van Roessel, P. and A. H. Brand. 2002. Imaging into the future: visualizing gene expression and protein interactions with fluorescent proteins. *Nat. Cell Biol.* 4:E15-20.
71. Vaupel, P., F. Kallinowski, and P. Okunieff. 1989. Blood flow, oxygen and nutrient supply, and metabolic microenvironment of human tumors: a review. *Cancer Res.* 49:6449-6465.
72. Vazquez, M. J., B. Rodriguez, C. Zapatero, and D. G. Tew. 2003. Determination of phosphate in nanomolar range by an enzyme-coupling fluorescent method. *Anal. Biochem.* 320:292-298.
73. Verstraete, K. L., Y. De Deene, H. Roels, A. Dierick, D. Uyttendaele, and M. Kunnen. 1994. Benign and malignant musculoskeletal lesions: dynamic contrast-enhanced MR imaging—parametric “first-pass” images depict tissue vascularization and perfusion. *Radiology* 192:835-843.
74. Wu, X., H. Liu, J. Liu, K. N. Haley, J. A. Treadway, J. P. Larson, N. Ge, F. Peale, and M. P. Bruchez. 2003. Immunofluorescent labeling of cancer marker Her2 and other cellular targets with semiconductor quantum dots. *Nat. Biotechnol.* 21:41-46.
75. Xia, Z. and Y. Liu. 2001. Reliable and global measurement of fluorescence resonance energy transfer using fluorescence microscopes. *Biophys. J.* 81:2395-2402.
76. Yang, M., T. Chishima, X. Wang, E. Baranov, H. Shimada, A. R. Moossa, and R. M. Hoffman. 1999. Multi-organ metastatic capability of Chinese hamster ovary cells revealed by green fluorescent protein (GFP) expression. *Clin. Exp. Metastasis* 17:417-422.
77. Yang, M., S. Hasegawa, P. Jiang, X. Wang, Y. Tan, T. Chishima, H. Shimada, A. R. Moossa, and R. M. Hoffman. 1998. Widespread skeletal metastatic potential of human lung cancer revealed by green fluorescent protein expression. *Cancer Res.* 58:4217-4221.
78. Yoshida, D., K. Watanabe, M. Noha, H. Takahashi, A. Teramoto, and Y. Sugisaki. 2003. Anti-invasive effect of an anti-matrix metalloproteinase agent in a murine brain slice model using the serial monitoring of green fluorescent protein-labeled glioma cells. *Neurosurgery* 52:187-197.